

1 **Divergent climate feedbacks on winter wheat growing and dormancy periods as**  
2 **affected by sowing date in the North China Plain**

3 Fengshan Liu<sup>1,2</sup>, Ying Chen<sup>1,\*</sup>, Nini Bai<sup>1</sup>, Dengpan Xiao<sup>4</sup>, Huizi Bai<sup>4</sup>, Fulu Tao<sup>2,3,5</sup>,  
4 Quansheng Ge<sup>2,3</sup>

5 1. China National Engineering Research Center of JUNCAO Technology, Forestry  
6 College, Fujian Agriculture and Forestry University, Fuzhou 350002, China

7 2. Key Laboratory of Land Surface Pattern and Simulation, Institute of Geographic  
8 Sciences and Natural Resources Research, CAS, Beijing 100101, China;

9 3. College of Resources and Environment, University of Chinese Academy of Sciences,  
10 Beijing 100049, China

11 4. Institute of Geographical Sciences, Hebei Academy of Sciences, Shijiazhuang 050011,  
12 China

13 5. Natural Resources Institute Finland (Luke), Helsinki 00790, Finland

14

15 Author: Liu Fengshan, PhD, specialized in agricultural meteorology and regional climate  
16 change. E-mail: liufs.11b@ igsnr.ac.cn

17 \* Corresponding author

18

19 **Abstracts:** Crop phenology exerts measurable impacts on soil surface properties,  
20 biophysical processes, and climate feedbacks, particularly at local/regional scales.  
21 Nevertheless, the response of surface biophysical processes to climate feedbacks as  
22 affected by sowing date in winter wheat croplands has been overlooked, especially during  
23 winter dormancy. The dynamics of leaf area index (LAI), surface energy balance and

24 canopy temperature ( $T_c$ ) were simulated by modified SiBcrop model under two sowing  
25 date scenarios (Early Sowing: EP; Late Sowing: LP) at 10 stations in the North China  
26 Plain. The results showed that the SiBcrop with a modified crop phenology scheme well  
27 simulated the seasonal dynamic of LAI,  $T_c$ , phenology, and surface heat fluxes. Earlier  
28 sowing date had higher LAI with earlier development than later sowing date. But the  
29 response of  $T_c$  to sowing date exhibited opposite patterns during the dormancy and active  
30 growth periods: EP led to higher  $T_c$  (0.05 K) than LP in the dormancy period and lower  
31  $T_c$  (-0.2K) in the growth period. The highest difference (0.6 K) between EP and LP  
32 happened at the time when wheat was sown in EP but wasn't in LP. The higher LAI  
33 captured more net radiation with warming effect, but partitioned more energy into latent  
34 heat flux with cooling. The climate feedback of sowing date, which was more obvious in  
35 winter in the northern areas and in the growing period in the southern areas, was  
36 determined by the relative contributions of albedo-radiative process and  
37 partitioning-non-radiative process. The study highlight the surface biophysical process of  
38 land management in modulating climate.

39 **Key words:** sowing date, canopy temperature, phenology, leaf area index, winter wheat,  
40 land surface model, North China Plain

41

## 42 **1. Introduction**

43 Land-atmosphere interactions are key components of the climate system. The land  
44 cover and management changes have strong feedbacks with climate through surface  
45 biophysical and biochemical processes (Mahmood et al. 2014). Cropland surface  
46 characteristic had been and will continue to be changed through crop management, such  
47 as cropping system (Jeong et al. 2014; Cui et al. 2018), sowing date and phenology shifts  
48 (Sacks et al. 2011; Richardson et al. 2013), and cultivars selection (Seneviratne et al.  
49 2018), to keep high yield under climate change condition. The changed cropland  
50 properties further generate feedback to regional climate through surface energy  
51 partitioning and albedo ( $\alpha$ ) mechanisms (Cooley et al. 2005; Zhang et al. 2015). It is  
52 important to quantify the climate feedback of crop phenology for regional climate  
53 prediction and agriculture sustainable development.

54 There are evidences that crop phenology has been shifted substantially in the major  
55 cultivation areas worldwide (Sacks and Kucharik 2011; Tao et al. 2012; Tao et al. 2014;  
56 Liu et al. 2017). In the North China Plain (NCP), the dates of sowing, dormancy,  
57 re-greening, anthesis, and maturity in wheat system were changed by 1.5, 1.5, -1.1, -2.7,  
58 and -1.4 days/decade (a positive value indicates delay and a negative value indicates  
59 advance), respectively (Xiao et al. 2013). The vegetative stages (including periods from  
60 dormancy to re-greening, re-greening to anthesis) were shortened and reproductive stage  
61 was prolonged (Xiao et al. 2013). Global warming induced-higher temperature resulted in  
62 longer photosynthetic-active period but faster development rate and shorter growth stages.  
63 Crop management, including sowing date adjustment and varietal change, reduced the  
64 length of vegetative stage, but increased the length of reproductive stage (Liu et al. 2010;

65 Liu et al. 2018). The management induced phenology dynamics are intended to increase  
66 yield. The strategies adapting to warmer environment include adopting cultivars with  
67 higher accumulated growing degree days (GDD) and later planting. The prolonged  
68 grain-filling period of winter wheat benefits the accumulation of carbohydrates in grain  
69 (Reynolds et al. 2012; Liu et al. 2018), and the adjusted sowing date reduces the risks  
70 such as insect and viral infection, adverse meteorological conditions, and soil water  
71 depletion (Sacks et al. 2010). Model simulation indicated that yield increase of winter  
72 wheat was benefitted from cultivars renewal by 12.2-22.6% and fertilization management  
73 by 2.1-3.6%; climate change damaged yield by -15.0% for rain-fed type, in the NCP  
74 (Xiao et al. 2014).

75 The crop phenology affects the seasonal rhythm of surface greenness and energy and  
76 water exchanges in the boundary layer. For example, maize growth duration prolonged  
77 and reached maturity and senesced a couple of weeks later, and the maximum change can  
78 reach  $47 \text{ W m}^{-2}$  and  $-20 \text{ W m}^{-2}$  for latent heat flux ( $LH$ ) and sensible heat flux ( $SH$ ),  
79 respectively, when the NDVI is increased by 0.1 in the Agro-IBIS model (Bagley et al.  
80 2015). Earlier planting date and longer grain-filling period increased the  $LH$  by  $3 \text{ W m}^{-2}$ ,  
81 decreased  $SH$  by  $2.5 \text{ W m}^{-2}$  in June and enhanced the net radiation ( $R_n$ ) by  $1.2 \text{ W m}^{-2}$  in  
82 October by reducing the interval time from maturity to harvest in American Corn belt  
83 (Sacks and Kucharik 2011). The change of surface coverage also shown regional climate  
84 feedback. The increased spring surface greenness at farmland, due to the advanced  
85 re-greening stage of winter wheat (Xiao et al. 2013; Liu et al. 2017), significantly  
86 impacted the patterns of  $LH$  and  $SH$  and then the changes of moderate to light rainfall  
87 (Zhang et al. 2015). Harvest shifted the key influence factors of the radiative balance and

88 evaporative fraction from leaf area and soil-atmosphere temperature difference to soil  
89 moisture in U.S. winter wheat (Bagley et al. 2017), and a shift in radiative forcing with  
90 the potential to warm the atmosphere by 1~1.4 °C through declining *LH* in the NCP (Cho  
91 et al. 2014). The influence of phenology on climate feedback through surface biophysical  
92 process at local/regional scale is worthy of further studies (Liu et al. 2017).

93 Despite previous studies showed the critical role of crop phenology in surface  
94 energy and water balance, there is an important potential sensitive period that has been  
95 ignored in the winter wheat system. During the dormancy period in winter, aboveground  
96 canopy of winter wheat remained constant for more than 2 months (Xiao et al. 2013). In  
97 view of the close relationships between surface biophysical processes and aboveground  
98 canopy (Boisier et al. 2012; Chen et al. 2015; Liu et al. 2017), the length from sowing  
99 date to start of dormancy would be the determinant factor to surface biophysical process  
100 in winter where winter wheat widely distributed, such as NCP, Pacific Northwest (Wuest  
101 2010) and Southern Great Plains of USA (Bagley et al. 2017), Australia, and numerous  
102 countries surrounding the Mediterranean Sea (Mahdi et al. 1998; Schillinger 2011).  
103 Compared with other phenology dynamics, such as earlier re-greening stage (Xiao et al.  
104 2013; Zhang et al. 2013), longer reproductive period (Sacks and Kucharik 2011) and  
105 inter-cropping period (Cho et al. 2014; Bagley et al. 2017), the climate feedback of  
106 sowing date emerges gradually with crop development. Particularly, winter wheat grows  
107 faster in early stages and slower as winter approaches, smaller change in sowing date  
108 could lead to larger and longer climate feedback in dormancy period. Recognition of the  
109 impacts of sowing date on land surface characteristics and climate feedback would be  
110 beneficial to the understanding of human influence on climate change. Therefore, it is

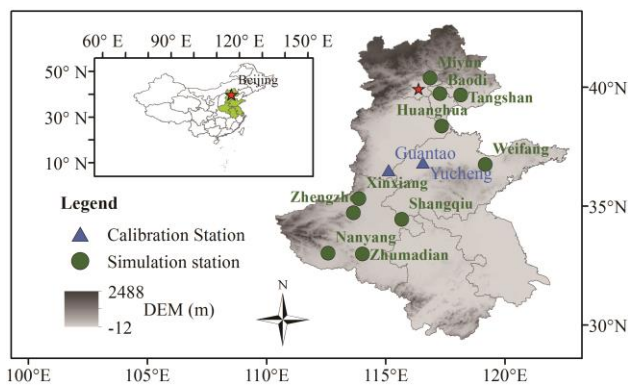
111 necessary to investigate whether dormancy period of winter wheat is sensitive to sowing  
112 date. And how sensitivities are surface biophysical process and climate effect?

## 113 2. Data and methods

### 114 2.1. Study stations

115 The NCP, with an area of  $4 \times 10^5 \text{ km}^2$ , is the largest winter wheat production region  
116 in China, including Hebei, Henan, Shandong, Jiangsu, and Anhui provinces, and Beijing  
117 and Tianjin municipalities (Fig.1). Summer maize - winter wheat rotation is the main  
118 cropping system, except Anhui and Jiangsu where winter wheat-rice rotation system is  
119 dominated. The satellite data showed a high cropland density above 70% with flat and  
120 relatively homogeneous agricultural practices (Liu et al. 2005; Ho et al. 2012). The soil  
121 type is classified as sandy loam according to the seven soil textures typified in the model  
122 (Sellers et al. 1996). Two stations with surface fluxes were used for model calibration  
123 (Fig.1, blue triangles). Ten randomly distributed stations with complete meteorology and  
124 phenology information were selected for simulation in this study (Fig.1, green dots). The  
125 details of fluxes, meteorology and phenology were further exhibited below.

126



127

128 **Fig.1** Distribution map of the study area and observation sites.

129 The 30 m resolution digital elevation model, provided by the GlobeLand30 in 2010, and  
 130 the administrative map were downloaded from the National Catalogue Service For  
 131 Geographic Information.

## 132 2.2 Data

### 133 2.2.1 Meteorology

134 The quality-controlled meteorological data, including air temperature ( $T_a$ ),  
 135 precipitation ( $P$ ), atmosphere pressure, relative humidity, and wind speed, was obtained  
 136 from the Chinese Meteorological Administration. Summer monsoon climate dominates  
 137 the region with an uneven distribution of annual precipitation (Table 1). In the 1980-2012,  
 138 the average annual  $P$  at the selected stations ranged between 550-990 mm, mainly  
 139 happened in summer. The mean yearly  $T_a$  varied between 11-15 °C. In the growing  
 140 season of winter wheat (11-12 and 1-6 month), the  $T_a$  varied between 7-11 °C among  
 141 stations and  $P$  ranged between 170-420 mm, which is consistent with the average climatic  
 142 conditions in the NCP (A et al. 2016). Climatological mean  $T_a$  and accumulated  $P$  during  
 143 the wheat growth period were calculated in the 10 stations and were linearly regressed  
 144 with the simulated differences between scenarios. Meteorological data was also used to  
 145 drive the model.

146 **Table 1** Climate conditions of the selected stations in 1980-2012

		Jan.	Feb.	Mar.	Apr.	May	Jun.	Jul.	Aug.	Sept.	Oct.	Nov.	Dec.	Average Wheat Season
$T_a$ (°C)	Miyun	-5.9	-2.2	4.8	13.5	19.6	24	25.8	24.5	19.3	12	3	-3.7	6.6
	Baodi	-5	-1.4	5.3	13.6	19.5	24	26.1	24.8	19.8	12.7	3.7	-2.7	7.1
	Tangshan	-4.8	-1.3	5.1	13.4	19.4	23.7	25.9	25	20.3	13	4.1	-2.5	7.1

	Huanghua	-3.4	-0.2	5.9	14.1	20.3	25	26.9	25.8	21.2	14.2	5.5	-1.2	8.3
	Weifang	-2.8	0.1	5.8	13.2	19.2	23.9	26.2	25.2	20.7	14.4	6.4	-0.3	8.2
	Xinxiang	0	3.3	8.7	15.8	21.2	25.8	27	25.9	21.3	15.3	7.9	1.8	10.6
	Zhengzhou	0.5	3.5	8.7	16	21.5	26	27.1	25.7	21.2	15.5	8.4	2.5	10.9
	Shangqiu	0.1	3.1	8.3	15.1	20.6	25.4	26.9	25.7	21.1	15.3	8.1	2	10.3
	Nanyang	1.6	4.4	9.1	15.8	21.2	25.5	27	26	21.7	16.1	9.4	3.5	11.3
	Zhumadian	1.5	4.2	9	15.7	21.2	25.7	27.2	25.9	21.6	16.3	9.6	3.6	11.3
$P$ (mm)	Miyun	2.2	4	9.7	19.9	43.1	86.7	180.7	172.6	62.9	25.5	9.4	2.3	177.3
	Baodi	2.7	3.7	9	20.1	36.2	82.4	169.7	142.6	49.7	27.5	10.1	3.6	167.8
	Tangshan	3.5	4.1	9.4	22.4	47	83.2	169.7	154.3	50.8	28.2	9.5	3.4	182.5
	Huanghua	3.2	5.5	10.1	21.3	42.8	84.2	177.2	111.6	41.5	31	11.9	3.5	182.5
	Weifang	6	10.3	14.9	24.5	45.4	80	136.5	132.1	56.1	32.8	18.8	8.9	208.8
	Xinxiang	4.6	7.1	19.2	25	49.9	65	150	119.5	59.8	32	14.9	5	190.7
	Zhengzhou	9.6	12.4	27.1	30.9	63.6	67.8	146.6	134.7	75.6	40.5	21.1	9.1	241.6
	Shangqiu	14.3	16.3	29.3	33	65	85.2	166.8	144.8	68.5	38.2	23.4	12.7	279.2
	Nanyang	13.2	15.6	35.2	41.7	78.8	124.5	183.7	131.7	76.3	51.1	30	12.8	351.8
	Zhumadian	21.9	24.8	51	50.9	93	128.6	227.7	176.3	98.2	63.9	35.2	18.5	423.9

147  $T_a$  means air temperature, and  $P$  means precipitation.

## 148 2.2.2 Verification data

149 To verify the applicability of the model, surface flux data was collected from  
150 Yucheng and Guantao stations (Fig.1; Table 2). The two stations used the same eddy  
151 covariance instruments to measure the surface latent heat flux (LI7500, LI-COR Inc.,  
152 Lincoln, NE, USA) and sensible heat flux (CSAT-3, Campbell Scientific Inc., Logan, UT,  
153 USA), but at different heights (Yucheng:3.3 m; Guantao: 15.6 m). The post-processing  
154 software (Yucheng: Eddypro; Guantao: EdiRe) was used to process the raw data such as  
155 spike detection, lag correction of H<sub>2</sub>O/CO<sub>2</sub> relative to the vertical wind component, sonic



156 virtual temperature correction, coordinating rotation using the planar fit method,  
 157 corrections for density fluctuation (WPL-correction), and frequency response correction  
 158 (Liu et al. 2011). The REddyProc was used for gap-filling by method of the look-up table  
 159 and the mean diurnal variations method (Falge et al. 2001; Wutzler et al. 2018). More  
 160 details could be referred to (Lei et al. 2010; Liu et al. 2013). Totally 10 complete winter  
 161 wheat season flux data were used to validate the model (Table 2).

162 The meteorology conditions were also synchronously measured during flux  
 163 observation (Table 2). The measurement included  $T_a$ ,  $P$ , atmosphere pressure, relative  
 164 humidity, wind speed, and sunshine. These data was the inputs of the model. According  
 165 to the  $T_a$  and  $P$ , the meteorological conditions were similar between the 10 stations for  
 166 simulation and the two stations for calibration. More variables were observed at Yucheng  
 167 station, such as wheat phenology and leaf area index (LAI) and canopy temperature ( $T_c$ ).  
 168 The observed durations of phenology, LAI, and fluxes at Yucheng station were in  
 169 2003-2006, 2004-2006, and 2003-2010, respectively.

170 **Table 2** General information about model verification data

Station	Period	Wheat growing season		Measured variables
		$T_a$ (°C)	$P$ (mm)	
Yucheng	2003-2010	9	226.7	Meteorology, Phenology, LAI, $LH$ , $SH$ , $T_c$
Guantao	2008-2010	9.6	134.4	Meteorology, $LH$ , $SH$

171  $T_a$  means air temperature,  $P$  means precipitation, LAI means leaf area index ( $m^2 m^{-2}$ ),  
 172  $LH$  means latent heat flux ( $W m^{-2}$ ),  $SH$  means sensible heat flux ( $W m^{-2}$ ).  $T_c$  means the  
 173 simulated canopy temperature (°C).

174

175 **2.2.3 Phenology of winter wheat**

176 The phenology information was obtained from China agro-meteorological  
177 experiment stations and available in the period of 1981-2009, except for 2003 at  
178 Zhumadian and 1986 and 1988 at Miyun station (Table 3). Phenological statistics showed  
179 that the sowing time of winter wheat is generally between DOY (Day Of Year) 270-290  
180 (early and middle October) in the NCP. After sowing, it generally takes about 6-10 days  
181 for germination. Winter wheat dormancy stage generally begins in DOY 330-360  
182 (December) and ends in DOY 40-70 (late February and early March), and reaches  
183 maturity in DOY 150-160(mid-June). The standard deviation shows that the inter-annual  
184 fluctuations of dormant and re-greening period is larger, and harvest period is relatively  
185 stable.

186 For the past 30 years, winter wheat phenology at some stations showed a significant  
187 linear trend (Table 4). The sowing and germination periods were significantly delayed in  
188 4 out of 10 stations, and the trend in the dormant and re-greening period was not obvious.  
189 Winter wheat matured significantly earlier at five stations. Generally, the autumn and  
190 winter phenophases, including sowing, germination and dormancy, are mainly delayed,  
191 while spring and summer phenophases, including re-greening and maturity, are primarily  
192 advanced. According to the fitting coefficient (a), the duration was changed by 5.7, 8.1,  
193 4.9, -3.5, and -5.5 in the period of 1981-2009, respectively, for the stages of sowing,  
194 germination, dormancy, re-greening and maturity of winter wheat. These results were  
195 consistent with our previous studies (Tao et al. 2012; Xiao et al. 2013; Xiao et al. 2015).

196

197 **Table 3** General information on the phenology of winter wheat in the selected stations  
198 (unit: DOY)

Station	Period	Sowing	Germination	Dormancy	Re-greening	Maturity
Miyun	1981-2009	275.52±7.55	284.96±9.03	331.93±6.41	73.59±15.1	168.26±3.46
Baodi	1981-2009	272.83±4.33	281.55±5.5	335.62±6.86	59.19±42.72	165.97±2.57
Tangshan	1981-2009 (except 2003)	271.86±4.83	279.59±6.04	335.55±6.6	66.62±7.98	169.97±3.23
Huanghua	1981-2009	274.17±7.83	280.32±7.03	340.38±8.65	62.45±6.56	157.14±3.25
Weifang	1981-2009	274.1±5.75	284.62±17.93	343.72±7.76	59.59±7.29	160.41±3.42
Xinxiang	1981-2009	283.59±4.21	291.64±5.14	351.9±10.56	47.55±7.16	152.03±3.3
Zhengzhou	1981-2009	289.76±5.67	298.45±6.65	360.5±14.08	44.21±7.43	151.34±3.88
Shangqiu	1981-2009	287.59±4.07	295.31±4.79	359.21±32.4	47.03±6.43	151.59±2.99
Nanyang	1981-2009	297.21±7.81	306.83±9.03	7.54±14.64	48.22±8.9	149.21±4.99
Zhumadian	1981-2009 (except 1986, 1988)	289.54±9.33	298.29±11.11	5.46±10.35	49.15±6.84	146.21±4.76

199 the data was shown in average ± standard deviation.

200

201 **Table 4** Linear trends in winter wheat phenology

Station	Sowing		Germination		Dormancy		Re-greening		Maturity	
	a	p	a	p	a	p	a	p	a	p
Miyun	<b>0.62</b>	<b>0.00</b>	<b>0.69</b>	<b>0.00</b>	0.17	0.27	-0.51	0.15	<b>-0.20</b>	<b>0.01</b>
Baodi	<b>0.31</b>	<b>0.00</b>	<b>0.41</b>	<b>0.00</b>	0.14	0.36	-0.67	0.52	-0.05	0.35
Tangshan	<b>0.41</b>	<b>0.00</b>	<b>0.51</b>	<b>0.00</b>	<b>0.43</b>	<b>0.00</b>	-0.29	0.11	<b>-0.20</b>	<b>0.00</b>
Huanghua	0.18	0.31	0.17	0.31	0.38	0.05	-0.07	0.64	-0.13	0.07
Weifang	0.20	0.11	0.61	0.13	0.11	0.55	0.14	0.38	-0.12	0.11

Xinxiang	0.07	0.46	0.12	0.34	0.27	0.26	-0.16	0.33	-0.12	0.10
Zhengzhou	-0.16	0.21	-0.21	0.17	-0.28	0.41	0.11	0.52	<b>-0.25</b>	<b>0.00</b>
Shangqiu	0.03	0.77	0.04	0.68	0.39	0.59	0.10	0.51	-0.07	0.28
Nanyang	-0.18	0.30	-0.11	0.60	-0.13	0.71	0.12	0.60	<b>-0.38</b>	<b>0.00</b>
Zhumadian	<b>0.49</b>	<b>0.02</b>	<b>0.56</b>	<b>0.02</b>	0.21	0.37	0.02	0.89	<b>-0.36</b>	<b>0.00</b>

202 a was the coefficient of linear fitting equation (d/year); p was the significance level;  
 203 bolded number means  $p < 0.05$ .

## 204 **2.3 Methods**

### 205 **2.3.1 Model calibration and verification**

206 The SiBcrop model was selected in this study. SiBcrop is a process-based land  
 207 surface model adapted from the Simple Biosphere model version 3 (Lokupitiya et al.  
 208 2009). The SiB series models (version 1, 2, 3 refers to SiB1, SiB2, SiB3, respectively) are  
 209 widely adopted land surface models for computing surface energy, water, momentum and  
 210 CO<sub>2</sub> exchange in the boundary layer. The SiBcrop version added the crop-specific  
 211 submodels of maize, soybean, winter and spring wheats, which was simple and detailed  
 212 enough in predicting LAI (Lokupitiya et al. 2009). The submodel replaces  
 213 remotely-sensed NDVI information by simulated LAI. SiBcrop simulated fast response  
 214 processes that vary sub-hourly such as energy, water, carbon and momentum balance of  
 215 the canopy and soil, as well as the processes that vary daily such as LAI. Surface energy  
 216 and water fluxes are calculated at each time step on a grid cell basis according to  
 217 physiologically based formulations of leaf-level photosynthesis, stomatal conductance  
 218 and respiration (Farquhar et al. 1980; Collatz et al. 1990).

219 The model was first modified according to the actual situation of winter wheat in the  
220 NCP (Chen et al. 2020). The SiBcrop model was originally calibrated in winter wheat –  
221 summer fallow system in which the growth time of wheat is relatively abundant  
222 (Lokupitiya et al. 2009). However, the NCP is dominated by winter wheat – summer  
223 maize system in which the development of wheat is strictly restricted. There are great  
224 differences in the varieties, planting date, growth environment and physiological  
225 characteristics of winter wheat between the two systems. The modifications include: (1)  
226 the sowing date was postponed to October from original August. (2) The cold tolerance  
227 was reduced to 8°C from original 18°C, above which the seven consecutive days for  
228 wheat sowing were counted. (3) The harsh condition of delayed sowing also reduced the  
229 daily growth rate, which was modified from 0.07 to 0.03 g m<sup>-2</sup> when GDD was 105-310  
230 °C d. (4) Wheat grows faster when GDD is 769-1074 °C d with maximum dry weight  
231 increased from 8 to 12 g and daily rate enlarged from 0.015 to 0.15 g m<sup>-2</sup>. (5) Specific  
232 leaf area was changed from 0.02 to 0.025 m<sup>2</sup> g<sup>-1</sup> (Najeeb et al. 2016). (6) A subroutine  
233 was added to describe the senescence process of canopy when GDD was larger than 1074  
234 °C d according to Tao et al (Tao et al. 2009). More details could be referred to Chen et al  
235 (2020).

236 After modifications, the simulated biases were within 10 days for wheat emergency  
237 and harvest dates, the determination coefficient, root mean square error, and agreement  
238 index between simulated and observed LAI were obviously improved from 0.26, 1.89 m<sup>2</sup>  
239 m<sup>-2</sup>, and 0.7 to 0.80, 0.99 m<sup>2</sup> m<sup>-2</sup>, and 0.91, respectively. And they were 0.66, 32.37 W  
240 m<sup>-2</sup>, and 0.84, respectively, for the simulated *LH* (Chen et al. 2020).

### 241 **2.3.2 Model simulation**

242 Two simulations with different sowing dates were performed to examine the  
243 responses of surface biophysical processes at the selected 10 stations (Fig.1). The  
244 planting date was classified into two scenarios: after DOY 265 (early sowing scenario,  
245 EP) and after DOY 275 (late sowing scenario, LP). The early and late sowing scenarios  
246 were established by artificially limiting the starting time of the sowing date. The early  
247 sowing scenario means that the sowing will not be allowed until DOY 265. Similarly, the  
248 late sowing scenario is only allowed after DOY 275. In both scenarios, wheat was sowed  
249 at the seventh consecutive days when temperature ranged 8~25°C, which means the real  
250 sowing date was seven days later. The winter wheat submodel in the SiBcrop was  
251 modified to be more cold tolerance (section 2.3.1), which caused the sowing date was less  
252 controlled by temperature. Therefore, the sowing dates were less constrained by climate  
253 difference among widely distributed stations. Our previous study showed that the delayed  
254 sowing date of winter wheat was mainly caused by the delayed harvest of maize (Xiao et  
255 al. 2013), which means the phenology of winter wheat was more affected by the previous  
256 crop than the climate in the NCP. The sowing dates in the two scenarios are within the  
257 climatological average of the region, indicating the reasonable choice of simulation  
258 scenarios.

259 The simulations were driven by the same meteorological data, initial condition, and  
260 soil texture from 1980 to 2009. The 1980-1984 was not analyzed as the spin-up time. The  
261 difference in the simulation results was mainly ascribed to the sowing date. The analyses  
262 focused on the dynamics of LAI and  $T_c$ , and the surface energy balance components such  
263 as  $R_n$ ,  $LH$ , and  $SH$ , which was used to explain the climate feedback mechanism.

### 264 **2.3.3. Methods to relate the surface energy balance components with $T_c$**

265 The Boisier method (Boisier et al. 2012) was adopted to relate the surface energy  
266 balance components with  $T_c$ . The energy partitioning of a terrestrial surface is expressed  
267 as

$$268 \quad (1-\alpha) S_d + L_d - L_u = LH + SH + R \quad (1)$$

269 Where  $S_d$ ,  $L_d$ , and  $L_u$  are the downward short-wave radiation, downward long-wave  
270 radiation, and upward long-wave radiation, respectively. In order to have a closed surface  
271 energy balance, the residual term  $R$  was derived explicitly from the other terms in  
272 equation (1), and principally accounts for the soil heat flux and canopy storage flux.

273 The  $T_c$  change simulated by model is affected by both radiative (surface albedo  
274 effect) and non-radiative processes (surface energy partitioning effect). In order to  
275 separate temperature variation caused by the sole change in absorbed short-wave  
276 radiation (radiative process), the following equation (Boisier et al. 2012) was used:

$$277 \quad \Delta T_c = (\varepsilon\sigma)^{-1/4} \left[ (L_u + \Delta L_u)^{1/4} - L_u^{1/4} \right] \quad (2)$$

278 Where  $\Delta T_c$  is the anomaly of canopy temperature (K). The  $\sigma$  is Stefan-Boltzmann  
279 constant ( $=5.67 \times 10^{-8} \text{ W m}^{-2} \text{ K}^{-4}$ ). The  $\varepsilon$  is surface emissivity ( $= 1$ ). A disturbance in  $S_d$ ,  
280  $L_d$ ,  $LH$ ,  $SH$  or  $R$  can be expressed as  $\Delta L_u$  by fixing non-perturbed terms using equation  
281 (1). More details can be found in Boisier et al. (2012).

282

## 283 **3 Results**

### 284 **3.1 SiBcrop simulation accuracy**

285 The simulation accuracy for  $T_c$  was analyzed by comparing the observation with  
286 simulation at Yucheng station over 2003-2010 (Supplement Fig.1). The linear regression  
287 equation (simulated  $T_c = 1.02 * \text{measured } T_c - 4.22$ ,  $R^2 = 0.91$ ,  $p < 0.001$ ) showed a good

288 linear relationship between the simulated  $T_c$  and the observed  $T_c$ . The coefficients of  
 289 linearly fitted equations indicating that the simulated  $T_c$  was slightly higher than the  
 290 measured (slope =1.02) and was negative deviated (intercept =-4.22).

291 The simulation error for wheat phenology at Yucheng station was within 10 days  
 292 (Chen et al. 2020). The sowing time under the two sowing scenarios was further  
 293 compared with observation at the selected 10 stations. The simulated sowing date was  
 294 stable, generally around  $DOY278.66 \pm 1.15$ , and  $DOY 290.34 \pm 2.08$  for EP and LP  
 295 scenario, respectively. The observed phenology fluctuated greatly. Wheat was prone to  
 296 sow later or early generally due to geographical location at some specific stations. In the  
 297 EP scenario, the stations in the north had a positive difference (delayed sowing date  
 298 relative to the actual date) compared to the actual phenological period, whereas the  
 299 stations in the south had a negative difference (advanced sowing date relative to the  
 300 actual date), because the stations in the north had earlier sowing date than those in the  
 301 south. In the LP scenario, the stations in the south were relatively close to the actual  
 302 phenology, but the stations near the north had a larger positive difference. Overall, the  
 303 simulation difference of phenology was within 15 days.

304 **Table 5** The difference between simulated and observed sowing dates under two  
 305 scenarios at each station

Station	Scenario	
	Early sowing	Late sowing
Miyun	4.19±7.82	17.48±7.55
Baodi	6.59±4.62	19.59±4.49



Tangshan	7.41±4.95	20.38±5.47
Huanghua	4.41±8.02	16.31±7.55
Weifang	4.34±5.6	15.86±5.55
Xinxiang	-5.31±4.24	5.59±4.24
Zhengzhou	-11.41±5.47	-0.38±5.53
Shangqiu	-9.34±3.84	1.48±3.85
Nanyang	-19.07±7.87	-8.41±8.08
Zhumadian	-11.36±8.91	-0.57±9.07
All	-2.98±10.96	8.7±11.66

---

306 data was show in average  $\pm$  standard deviation.

307

### 308 **3.2 Seasonal dynamics of LAI and $T_c$ in scenarios**

309 Wheat LAI curves for the two sowing dates were not overlapped (Fig.2a). The LAI  
310 in the EP scenario was larger with earlier development. With the sowing in the LP  
311 scenario, LAI difference between the two scenarios gradually narrowed until the spring of  
312 the next year when the disparity increased again (Fig.3a). The LAI difference between  
313 two scenarios had a valley after the reproductive period. With the approaching of harvest,  
314 the difference gradually decreased to 0.

315 The LAI difference of winter wheat in two scenarios is mainly attributed to the  
316 difference in the accumulation of biomass. In the EP scenario, earlier sowing means  
317 advanced assimilation process and better temperature conditions, more photosynthetic  
318 carbon was produced and distributed into leaf. The impact of sowing time on LAI

319 displayed great dissimilarity among stations (Fig.3a). Based on linear regression, the  
320 seasonal average of wheat LAI difference between scenarios was highly related with  
321 precipitation in the growth period ( $LAI\ anomaly = 0.0011 * P - 0.12$ ,  $R^2 = 0.59$ ). The  
322 more precipitation, the greater influence of sowing date on growth. The  $T_a$  contributed  
323 little to the LAI difference between the two scenarios.

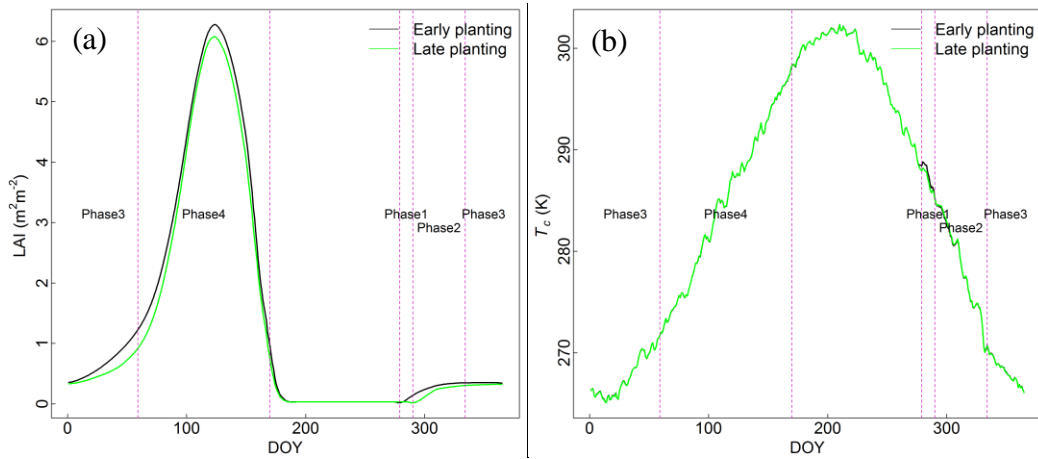
324 According to the  $T_c$  difference between scenarios, the following phenologies of  
325 winter wheat were relatively important: sowing date, dormancy date, re-greening date and  
326 maturity date. Based on the simulation results, the phenological dates used here as  
327 follows: EP sowing date, DOY279; LP sowing date, DOY290; dormancy date, DOY334;  
328 re-greening date, DOY59; maturity date, DOY170 (Fig.2a). The  $T_c$  difference between  
329 scenarios was separated into 4 phases: Phase 1, inter-sowing period, when wheat had  
330 been sown in the EP but hadn't in the LP; Phase 2: early growing period, from sowing  
331 date of LP to dormancy date; Phase 3: dormancy period, from dormancy date to  
332 re-greening date; Phased 4: late growing period, from re-greening date to maturity date  
333 (Fig.2b).

334 The most obvious disparity in  $T_c$  between two scenarios occurred in the inter-sowing  
335 period (Fig.2b). The development of early sown winter wheat resulted in higher  $T_c$ , with a  
336 peak of up to 0.6 K. The growth of wheat in the LP sharply reduced the warming effect in  
337 EP, and eventually the EP scenario had lower temperature (-0.2K) before entering the  
338 dormancy period. The temperature change process during this period was relatively  
339 consistent across the selected stations (Fig.3b). In the late growing period, the EP had  
340 lower temperature (-0.1 K) than LP. In particular, LAI difference varied greatly between  
341 stations (Fig.3a),  $T_c$  difference was relatively stable (Fig.3b).

342 Another special period is the dormancy period, when EP had higher  $T_c$  than LP with  
343 an average of 0.05 K (Fig.3b). With the start of the re-greening period, the EP  $T_c$  was  
344 gradually lower than LP  $T_c$  and dropped to 0 at the harvest time. The  $T_c$  dynamics during  
345 this period was highly heterogeneous among the stations, varying between -0.25~0.25 K.

346 In the dormancy period, the  $T_c$  anomaly between scenarios was significantly affected  
347 by the  $T_a$  in winter ( $T_c$  anomaly =  $-0.023 * T_a + 0.062$ ,  $R^2 = 0.6$ ,  $p = 0.005$ ). The lower the  
348  $T_a$ , the bigger the  $T_c$  difference, which indicating that the influence of sowing date is  
349 more important in northern farmland. The linear relationship between  $P$  and  $T_c$  difference  
350 in winter was not obvious. The linear fitting equation between  $P$  and  $T_c$  anomaly in the  
351 growing period:  $T_c$  anomaly =  $-0.0013 * P + 0.057$ ,  $R^2 = 0.8$ ,  $p < 0.001$ . More rainfall  
352 increased the  $T_c$  anomaly in the growing period. The linear fitting equation between  $T_a$   
353 and  $T_c$  anomaly in the growing period:  $T_c$  anomaly =  $-0.017 * T_a + 0.2$ ,  $R^2 = 0.53$ ,  $p =$   
354  $0.01$ . Since the  $T_c$  anomaly was negative, the higher the  $T_a$ , the greater the  $T_c$  anomaly.  
355 Considering the low temperature and less precipitation at the northern stations, the high  
356 temperature and more precipitation at the southern stations, the climate feedback of  
357 sowing date was more obvious in winter in the northern areas, and in the growing period  
358 in the southern areas.

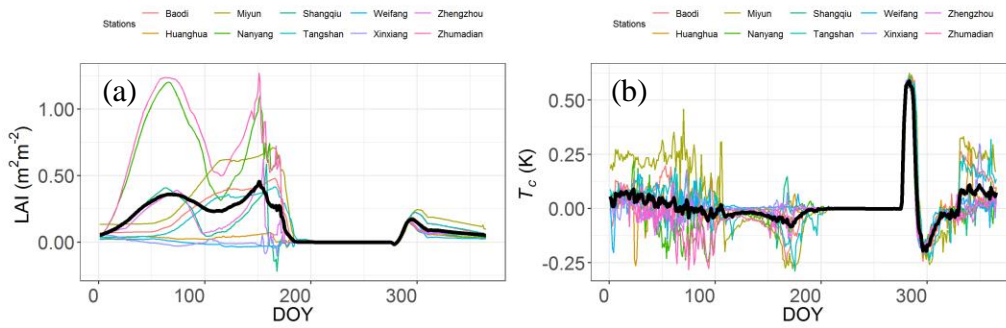
359



360 **Fig.2** Dynamics of (a) LAI and (b)  $T_c$  under two sowing scenarios in winter wheat

362 growing season

363 Phase 1: inter-sowing period, when wheat had been sown in the EP but hadn't in the  
 364 LP; Phase 2: early growing period, from sowing date of LP to dormancy date; Phase 3:  
 365 dormancy period, from dormancy date to re-greening date; Phased 4: late growing period,  
 366 from re-greening date to maturity date.



367 **Fig.3** Seasonal differences in (a) LAI and (b)  $T_c$  of EP-LP at each station. The  
 368 average across the stations was shown in bold black line

370

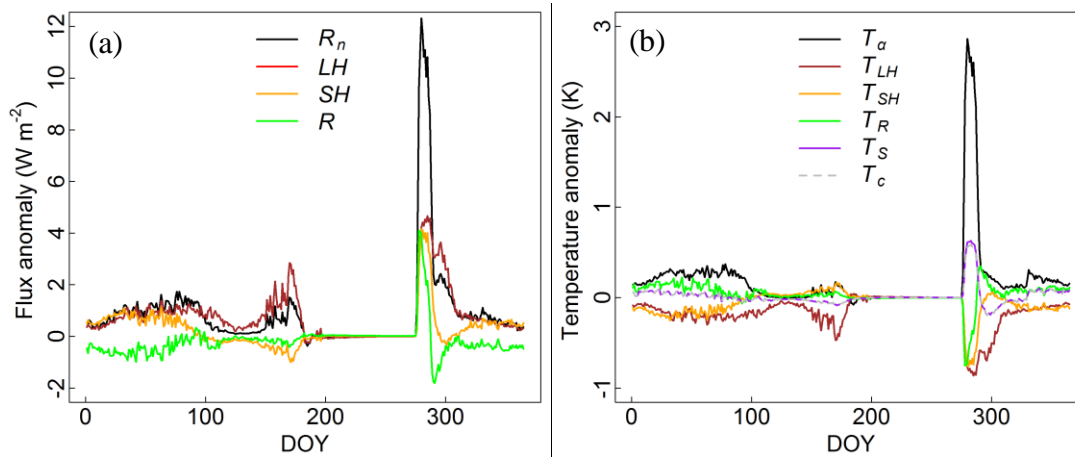
371

372 **3.3 Contributions of surface energy balance components to scenario difference in  $T_c$**

373 According to the seasonal dynamics of LAI and  $T_c$ , winter wheat growth could not  
374 explain the difference in climate effect of sowing time. Specifically, the  $T_c$  anomaly  
375 between the two scenarios was reversed between the dormancy (Phase 3) and active  
376 growth periods (Phase 2 and Phase 4), but with both positive LAI difference (Fig.3). In  
377 this section, surface energy balance was used to explain the response of  $T_c$  to sowing  
378 date.

379 The flux anomalies of  $R_n$ ,  $LH$ ,  $SH$  and  $R$  were shown in Fig.4a. The EP scenario  
380 always maintained higher  $R_n$  and  $LH$ . Especially winter wheat-covered ground captured  
381 more than  $10 \text{ W m}^{-2}$   $R_n$  than bare land. The anomaly of  $R_n$  in different sowing dates was  
382 maintained within  $2 \text{ W m}^{-2}$ .  $LH$  generally was covariant with the change in  $R_n$ . However,  
383 the anomaly of  $LH$  in the late growth period was greater than that of  $R_n$ , resulting in  
384 negative  $SH$ , indicating that the EP scenario had stronger  $LH$  distribution tendency and  
385 less  $SH$  was partitioned. Bigger anomaly of  $SH$  was happened in the initial and dormant  
386 stages.  $R$  anomaly fluctuated obviously only in the initial phase.

387 The contributions of surface energy balance components to  $T_c$  were shown in Fig.4b.  
388 Stronger radiation absorption provided more energy for the thermal motion of air and  
389 causing positive  $T_c$  differences of EP-LP. Correspondingly, higher distribution into  $LH$ ,  
390  $SH$ , and  $R$  was conducive to cooling  $T_c$ . Therefore, positive  $LH$  and  $SH$  differences of  
391 EP-LP showed negative  $T_c$  effects, and negative  $R$  difference of EP-LP showed positive  
392  $T_c$  effect. The positive  $T_c$  anomaly of EP-LP reflected that the radiative process played the  
393 major role in the dormancy period. In the active growth time, the cooling effect of  $LH$   
394 partitioning dominated the  $T_c$  anomaly.



395 **Fig.4** (a) The differences in the surface fluxes between the sowing scenarios of EP  
 396 and LP, (b) its contributions to  $T_c$  anomaly.

397

398  $R_n$  means net radiation,  $T_a$  represents the temperature anomaly induced by changes  
 399 in absorbed solar radiation.  $T_{LH}$  represents the temperature anomaly induced by changes  
 400 in latent flux.  $T_{SH}$  represents the temperature anomaly induced by changes in sensible flux.  
 401  $T_R$  represents the temperature anomaly induced by changes in residual term.  $T_S$  represents  
 402 the temperature anomaly induced by changes in solar radiation, latent, sensible and  
 403 residual fluxes.

404

## 405 **4 Discussion**

### 406 **4.1 The diverse trends in sowing date of winter wheat in the NCP**

407 The spatiotemporal changes of winter wheat phenology had been extensively  
 408 examined in the NCP. In the period of 1981-2009, the sowing date was on average  
 409 delayed by 1.5 days/decade, but 8 out of the 36 agro-meteorological experiment stations  
 410 were advanced (Xiao et al. 2013). The diverse trends in sowing date were also existed at  
 411 the national scale, where 6 stations significantly advanced by up to 9.1 days/decade, and  
 412 11 stations significantly delayed by up to 10 days/decade (Tao et al. 2012).

413 The main reasons for crop phenology include climate warming and variety renewal  
414 (Mirschel et al. 2005; Eyshi Rezaei et al. 2017; Liu et al. 2017). Climate warming mainly  
415 leads to the delay of sowing date, and variety renewal is more likely to affect the length  
416 of reproductive period. The management practices, photoperiod, and the time of summer  
417 maize harvest also contributed to the shift of winter wheat sowing date (Yuan et al. 2010).

418 The proper sowing date is key to ensure winter wheat survive through winter and  
419 reduce the freezing injury, insect pests and other harmful conditions (Sacks et al. 2010;  
420 Zhang et al. 2012; Newbery et al. 2016). With faster growth in warmer environment, the  
421 sowing date should be postponed to maintain a proper coverage of winter wheat in  
422 dormancy period. The warming of the NCP is regionally consistent (Shi et al. 2014), and  
423 the diverse change of sowing date will affect the coverage of winter wheat, especially one  
424 fifth stations advanced their sowing date. Earlier sowing may also benefited from the  
425 reduction in freezing damage and the increase in pest diseases caused by higher minimum  
426 temperature, since more above-ground biomass will not be subject to lethal freezing  
427 damage and will resist higher harms from pests and diseases. There are also management  
428 practices to counteract the effects of advanced sowing date, such as deep tillage and  
429 delayed irrigation, which reduce the development of leaves and stems. Until now, fewer  
430 studies had focused on the phenomenon of early sowing date and its underlying causes  
431 and countermeasures.

432 Sowing date significantly affected land surface characteristic. There were several  
433 times of differences in surface coverage between two sowing dates (Supplement Fig.2).  
434 Differences in spectral characteristics, canopy structure and physiological activities  
435 between soil and winter wheat can significantly affect surface biophysical processes such

436 as surface reflectivity, roughness, canopy resistance and surface energy budget  
437 (Richardson et al. 2013). In this study, the two sowing scenarios showed clear disparity in  
438 LAI (Fig.2a).

#### 439 **4.2 Warming effect of EP-LP in the dormancy period**

440 Although there were literatures reporting that the albedo process in winter is  
441 relatively important (Richardson et al. 2013; Lombardozzi et al. 2018), fewer studies  
442 directly addressed the influence of different surface characteristics and climate effect  
443 through biophysical process in the dormancy period. In the Oklahoma's winter wheat belt,  
444 the rapid crop growth during November exhibited a distinct cool anomaly against  
445 adjacent regions of dormant grassland. Over the period of December through April, the  
446 cool bias was visibly diminished although the greenness difference between grassland  
447 and wheat was more distinct (McPherson et al. 2004). The biophysical impacts between  
448 maize and perennial grass were simulated using Agro-IBIS model in US corn belt  
449 (Bagley et al. 2015). The results showed that much higher LAI of perennial scenario was  
450 existed in winter December–February ( $3$  vs  $0 \text{ m}^2 \text{ m}^{-2}$ ) and in summer June–August ( $10$  vs  
451  $4 \text{ m}^2 \text{ m}^{-2}$ ). Perennial grass had smaller surface albedo (coupling snow effect) than maize  
452 in winter, but showed quite small difference in summer. During winter and summer, the  
453 perennial scenario had slightly higher  $LH$  than the maize scenario, but the difference in  $R_n$   
454 between two scenarios was more than  $10 \text{ W m}^{-2}$  in winter (Bagley et al. 2015). The above  
455 studies indicated that the cooling effect of higher LAI was inhibited in winter. The results  
456 of this current study indicate that higher LAI in winter has a warming effect. The main  
457 reason was due to the relative contributions of surface albedo mechanism and surface flux  
458 distribution process.

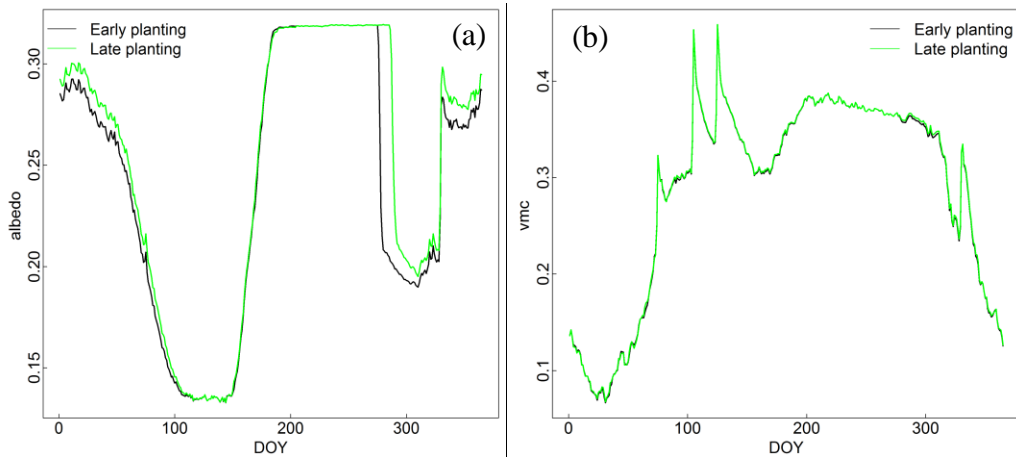


459 The simple increased crop coverage on the bare ground would substantially alter  
460 surface albedo results from the decreasing contribution of the soil to the canopy  
461 reflectance (Hammerle et al. 2008). In the SiBcrop model, the reflectivity of different  
462 surface coverings varies greatly in the visible band (Table 6). The germination of winter  
463 wheat immediately changed the bare soil into soil with crop, which is favorable to the  
464 sharp reduction after crop covered. The measured surface albedo in winter could drop to  
465 0.14 (Liu et al. 2019). The surface albedo was computed based on surface energy budget  
466 at Weishan station, the bare ground albedo can be higher than 0.3 and the winter wheat  
467 lower than 0.15 (data not shown). Therefore, early sowing in EP scenario results in higher  
468 LAI, which can significantly affect the surface albedo at the initial stage and continuously  
469 have a lower albedo than that in LP scenario. The effect of the soil on the canopy  
470 reflectance is negligible at  $LAI > 2 \text{ m}^2 \text{ m}^{-2}$  (Goudriaan 1977), which explained why the  
471  $R_n$  anomaly of EP-LP was small after the re-greening stage. In the model, the senescence  
472 of winter wheat is a process in which LAI decreases rapidly, and the disparity in LAI  
473 variations between the two scenarios further led to the difference in surface albedo and  $R_n$   
474 during the late growth period.

475 The strong climate feedback in inter-sowing period, when wheat had been sown in  
476 the EP but hadn't in the LP, was related to the effect of tillage on maize stubble. The  
477 NCP is dominated by summer maize - winter wheat rotation system in which the ground  
478 is covered with maize stubble before wheat is sown. The damage of sowing to stubble is  
479 conducive to the reduction of albedo since stubble has larger surface reflectivity than soil  
480 (O'Brien et al. 2019). The 0.1 increase of surface albedo caused by no-till management,  
481 which was also the magnitude of our simulation (Table 6), cooling the hottest summer

482 days by 2 °C or more (Davin et al. 2014). The inter-sowing period is equivalent to  
483 no-tillage period, when early sowed wheat absorbed more net radiation with lower albedo  
484 by destroying stubble and causing higher temperature (Fig.3b, Fig4a).

485 Previous studies showed that the increase of vegetation cover caused warming  
486 feedback by destroying the high albedo of snow in the case of snow cover (Richardson et  
487 al. 2013; Bagley et al. 2015; Lombardozzi et al. 2018). In our simulation, except for the  
488 large difference in crop coverage in phase 1, the snow and crop had consistent coverage  
489 in other phases (Supplement Table 1), which means albedo difference between two  
490 scenarios was not caused by snow. Low soil water content contributed to the high surface  
491 albedo (Seneviratne et al. 2010)(Fig.5b). With the decrease of surface soil moisture,  
492 surface albedo increased in winter, which explained why albedo in the winter was higher  
493 than that in the growth period. The increase in soil reflectivity caused by soil drying  
494 enhanced the role of low winter wheat reflectivity in surface albedo, the albedo disparity  
495 between the two scenarios increased in winter, which strengthened the albedo-radiative  
496 mechanism. Low soil moisture also contributed to the disparity in warming effect  
497 between EP and LP during dormancy period (Fig.5b). The lack of precipitation in winter  
498 made soil moisture unable to be replenished effectively, thus reducing soil evaporation  
499 and crop transpiration. But during the growing season, soil moisture is high enough to  
500 supply transpiration. The lower the  $T_a$ , the lower the transpiration vitality, thus unable to  
501 offset the warming effect of increased  $R_n$  absorption, which explained why the winter  $T_c$   
502 disparity among stations was controlled by  $T_a$ .



503 **Fig.5** Dynamics of (a) surface albedo and (b) surface soil moisture content under two  
 504 sowing scenarios in winter wheat growing season  
 505

506

507 **Table 6** The reflectivity of different surface coverings in near-infrared and visible bands  
 508 in the SiBcrop model

Material	Visible band	Near Infrared band
Green leaf	0.08	0.3
Snow	0.8	0.4
Soil with crop	0.11	0.314
Bare soil	0.33	0.35

509

### 510 **4.3 Cooling effect of EP-LP during the growing period**

511 The phenological shifts, such as earlier leaf unfolding, delayed leaf fall, and  
 512 lengthening of the green-cover season have feedback on climate through biophysical and  
 513 biogeochemical processes (Penuelas et al. 2009). Previous studies showed cooling effect  
 514 in the photosynthetic active period through surface biophysical mechanism in the  
 515 cropland (e.g. (Sacks and Kucharik 2011; Zhang et al. 2013; Bohm et al. 2020)).

516 In the NCP, the increased spring surface greenness at farmland, benefited from  
517 advanced re-greening stage of winter wheat (Xiao et al. 2013; Liu et al. 2017), had  
518 cooling and wetting effects (Zhang et al. 2013) and suppressed the moderate to light  
519 rainfall (Zhang et al. 2015). The analysis found that surface greening increased the  
520 partitioning into  $LH$  and reduced  $SH$  to cooling surface air and suppression of rainfall  
521 (Zhang et al. 2013; Zhang et al. 2015). Distinguished difference between early-covering  
522 crops (winter wheat, winter rapeseed, winter barley) and late-covering crops (corn, silage  
523 maize, sugar beet) in central Europe caused impacts on simulated surface energy fluxes  
524 and temperature in the Noah-MP model, the higher LAI led to an increase in  $LH$ ,  
525 decreased in  $SH$  and eventually surface cooling in May-September (Bohm et al. 2020).  
526 The Agro-IBIS model was used to study the impacts on surface energy balance of  
527 advanced corn sowing date (10 days): Early sowing means earlier development and  
528 senescence of LAI, causing stronger disparity of  $LH$  than  $R_n$  with bigger LAI and  
529 probably a slight cooling of  $T_a$  in June (Sacks and Kucharik 2011). Similar conclusions  
530 were presented based on simulated  $T_c$  results with modified SiBcrop.

531

## 532 **5 Conclusions**

533 The dynamics of winter wheat LAI and  $T_c$  under two sowing date scenarios were  
534 simulated by the SiBcrop model in the NCP, and the  $T_c$  disparity between the two  
535 scenarios was explained by the surface energy balance. The findings include:

536 (1) Earlier sowing date of winter wheat had higher LAI than later sowing date.

537 (2) The  $T_c$  disparity between EP and LP is divided into two periods: warming effect  
538 in the dormancy period, and cooling effect in the active growth period.

539 (3) Surface energy balance can interpret the climate feedback mechanism of sowing  
540 date, that is, the dominated role of albedo-radiative process in the dormancy period is  
541 surpassed by  $LH$  partitioning-non-radiative process in the growth period.

542 (4) The responses of LAI and  $T_c$  to sowing date at station scale were divergent:  
543 controlled by  $T_a$  in the dormancy period, and influenced by  $P$  and  $T_a$  in the growth period.

544 The study had some shortcomings. The single model simulation was highly  
545 dependent on the structure and parameterization scheme of the model. The climate  
546 feedback was reflected by the canopy temperature. In the SiBcrop model, the spatial  
547 distribution of stations was not fully considered in the determination of sowing date,  
548 which resulted in too early or too late sowing at some stations. Nevertheless, the study  
549 highlighted the divergent climate feedbacks on winter wheat dormancy as affected by  
550 sowing date. The simulation error of sowing date in land surface models is commonly  
551 higher than 10 days (Song et al. 2013; Chen et al. 2020), which may produce detectable  
552 climate effect especially in northern winter and then misestimate the variation of  
553 minimum temperature. The crop management changes as a potential way should be  
554 considered in mitigating climate warming. In the cold dry north, delayed sowing and  
555 reduced irrigation would alleviate the temperature increase in winter, whereas in south  
556 with better hydrothermal conditions, enhanced vegetation coverage would be beneficial.

557

### 558 **Acknowledgments**

559 This study is supported by the National Natural Science Foundation of China  
560 (41801020).

561

562 **References**

- 563 A, D., Xiong, K., Zhao, W., Gong, Z., Jing, R., and Zhang, L.: Temporal trend of climate  
564 change and mutation analysis of North China Plain during 1960 to 2013. *Scientia*  
565 *Geographica Sinica*, 36(10), 1555-1564, 2016.
- 566 Bagley, J. E., Kueppers, L. M., Billesbach, D. P., Williams, I. N., Biraud, S. C., and Torn,  
567 M. S.: The influence of land cover on surface energy partitioning and evaporative fraction  
568 regimes in the US Southern Great Plains. *Journal of Geophysical Research-Atmospheres*,  
569 122(11), 5793-5807, 2017.
- 570 Bagley, J. E., Miller, J., and Bernacchi, C. J.: Biophysical impacts of climate - smart  
571 agriculture in the Midwest United States. *Plant, cell & environment*, 38(9), 1913-1930,  
572 2015.
- 573 Bohm, K., Ingwersen, J., Milovac, J., and Streck, T.: Distinguishing between early- and  
574 late-covering crops in the land surface model Noah-MP: impact on simulated surface  
575 energy fluxes and temperature. *Biogeosciences*, 17(10), 2791-2805, 2020.
- 576 Boisier, J. P., de Noblet-Ducoudre, N., Pitman, A. J., Cruz, F. T., Delire, C., van den  
577 Hurk, B. J. J. M., et al.: Attributing the impacts of land-cover changes in temperate  
578 regions on surface temperature and heat fluxes to specific causes: Results from the first  
579 LUCID set of simulations. *Journal of Geophysical Research-Atmospheres*, 117, 2012.
- 580 Chen, M., Griffis, T. J., Baker, J., Wood, J. D., and Xiao, K.: Simulating crop phenology  
581 in the Community Land Model and its impact on energy and carbon fluxes. *Journal of*  
582 *Geophysical Research-Biogeosciences*, 120(2), 310-325, 2015.
- 583 Chen, Y., Liu, F., Tao, F., Ge, Q., Jiang, M., Wang, M., et al.: Calibration and validation  
584 of SiBcrop Model for simulating LAI and surface heat fluxes of winter wheat in the  
585 North China Plain. *Journal of Integrative Agriculture*, 19(9), 2-11, 2020.
- 586 Cho, M. H., Boo, K. O., Lee, J., Cho, C., and Lim, G. H.: Regional climate response to  
587 land surface changes after harvest in the North China Plain under present and possible  
588 future climate conditions. *Journal of Geophysical Research-Atmospheres*, 119(8),  
589 4507-4520, 2014.
- 590 Collatz, G. J., Berry, J. A., Farquhar, G. D., and Pierce, J.: The relationship between the  
591 Rubisco reaction mechanism and models of photosynthesis\*. *Plant, Cell & Environment*,  
592 13(3), 219-225, 1990.
- 593 Cooley, H. S., Riley, W. J., Torn, M. S., and He, Y.: Impact of agricultural practice on  
594 regional climate in a coupled land surface mesoscale model. *Journal of Geophysical*  
595 *Research Atmospheres*, 110(D03113, doi:10.1029/2004JD005160.), -, 2005.
- 596 Cui, J., Yan, P., Wang, X., Yang, J., Li, Z., Yang, X., et al.: Integrated assessment of  
597 economic and environmental consequences of shifting cropping system from  
598 wheat-maize to monocropped maize in the North China Plain. *Journal of Cleaner*  
599 *Production*, 193, 524-532, 2018.
- 600 Davin, E. L., Seneviratne, S. I., Ciais, P., Olliso, A., and Wang, T.: Preferential cooling  
601 of hot extremes from cropland albedo management. *Proceedings of the National*  
602 *Academy of Sciences of the United States of America*, 111(27), 9757-9761, 2014.
- 603 Eyshi Rezaei, E., Siebert, S., and Ewert, F.: Climate and management interaction cause  
604 diverse crop phenology trends. *Agricultural and Forest Meteorology*, 233, 55-70, 2017.

605 Falge, E., Baldocchi, D., Olson, R., Anthoni, P., Aubinet, M., Bernhofer, C., et al.: Gap  
606 filling strategies for defensible annual sums of net ecosystem exchange. *Agricultural and*  
607 *Forest Meteorology*, 107(1), 43-69, 2001.

608 Farquhar, G. D., von Caemmerer, S., and Berry, J. A.: A biochemical model of  
609 photosynthetic CO<sub>2</sub> assimilation in leaves of C<sub>3</sub> species. *Planta*, 149(1), 78-90, 1980.

610 Goudriaan, J. 1977. *Crop micrometeorology : a simulation study*, Pudoc.

611 Hammerle, A., Haslwanter, A., Tappeiner, U., Cernusca, A., and Wohlfahrt, G.: Leaf area  
612 controls on energy partitioning of a temperate mountain grassland. *Biogeosciences*, 5(2),  
613 421-431, 2008.

614 Ho, C.-H., Park, S.-J., Jeong, S.-J., Kim, J., and Jhun, J.-G.: Observational Evidences of  
615 Double Cropping Impacts on the Climate in the Northern China Plains. *Journal of*  
616 *Climate*, 25(13), 4721-4728, 2012.

617 Jeong, S.-J., Ho, C.-H., Piao, S., Kim, J., Ciais, P., Lee, Y.-B., et al.: Effects of double  
618 cropping on summer climate of the North China Plain and neighbouring regions. *Nature*  
619 *Clim. Change*, 4(7), 615-619, 2014.

620 Lei, H., Yang, D., Lokupitiya, E., and Shen, Y.: Coupling land surface and crop growth  
621 models for predicting evapotranspiration and carbon exchange in wheat-maize rotation  
622 croplands. *Biogeosciences*, 7(10), 3363-3375, 2010.

623 Liu, C., Gao, Z., Li, Y., Gao, C. Y., Su, Z., and Zhang, X.: Surface Energy Budget  
624 Observed for Winter Wheat in the North China Plain During a Fog–Haze Event.  
625 *Boundary-Layer Meteorology*, 170(3), 489-505, 2019.

626 Liu, F., Chen, Y., Shi, W., Zhang, S., Tao, F., and Ge, Q.: Influences of agricultural  
627 phenology dynamic on land surface biophysical process and climate feedback. *Journal of*  
628 *Geographical Sciences*, 27(9), 1085-1099, 2017.

629 Liu, J., Liu, M., Tian, H., Zhuang, D., Zhang, Z., Zhang, W., et al.: Spatial and temporal  
630 patterns of China's cropland during 1990–2000: An analysis based on Landsat TM data.  
631 *Remote Sensing of Environment*, 98(4), 442-456, 2005.

632 Liu, S., Xu, Z., Zhu, Z., Jia, Z., and Zhu, M.: Measurements of evapotranspiration from  
633 eddy-covariance systems and large aperture scintillometers in the Hai River Basin, China.  
634 *Journal of Hydrology*, 487, 24-38, 2013.

635 Liu, S. M., Xu, Z. W., Wang, W. Z., Jia, Z. Z., Zhu, M. J., Bai, J., et al.: A comparison of  
636 eddy-covariance and large aperture scintillometer measurements with respect to the  
637 energy balance closure problem. *Hydrology and Earth System Sciences (HESS) &*  
638 *Discussions (HESSD)*, 15, 1291-1306, 2011.

639 Liu, Y. A., Wang, E. L., Yang, X. G., and Wang, J.: Contributions of climatic and crop  
640 varietal changes to crop production in the North China Plain, since 1980s. *Global Change*  
641 *Biology*, 16(8), 2287-2299, 2010.

642 Liu, Y. J., Chen, Q. M., Ge, Q. S., Dai, J. H., Qin, Y., Dai, L., et al.: Modelling the  
643 impacts of climate change and crop management on phenological trends of spring and  
644 winter wheat in China. *Agricultural and Forest Meteorology*, 248, 518-526, 2018.

645 Liu, Z., Wu, C., Liu, Y., Wang, X., Fang, B., Yuan, W., et al.: Spring green-up date  
646 derived from GIMMS3g and SPOT-VGT NDVI of winter wheat cropland in the North  
647 China Plain. *Isprs Journal of Photogrammetry & Remote Sensing*, 130, 81-91, 2017.

648 Lokupitiya, E., Denning, S., Paustian, K., Baker, I., Schaefer, K., Verma, S., et al.:  
649 Incorporation of crop phenology in Simple Biosphere Model (SiBcrop) to improve  
650 land-atmosphere carbon exchanges from croplands. *Biogeosciences*, 6(6), 969-986, 2009.

651 Lombardozi, D. L., Bonan, G. B., Wieder, W., Grandy, A. S., Morris, C., and Lawrence,  
652 D. M.: Cover Crops May Cause Winter Warming in Snow - Covered Regions.  
653 *geophysical research letters*, 45(18), 9889-9897, 2018.

654 Mahdi, L., Bell, C. J., and Ryan, J.: Establishment and yield of wheat (*Triticum turgidum*  
655 L.) after early sowing at various depths in a semi-arid Mediterranean environment. *Field*  
656 *Crops Research*, 58(3), 187-196, 1998.

657 Mahmood, R., Pielke, R. A., Hubbard, K. G., Niyogi, D., Dirmeyer, P. A., McAlpine, C.,  
658 et al.: Land cover changes and their biogeophysical effects on climate. *International*  
659 *Journal of Climatology*, 34(4), 929-953, 2014.

660 McPherson, R. A., Stensrud, D. J., and Crawford, K. C.: The Impact of Oklahoma's  
661 Winter Wheat Belt on the Mesoscale Environment. *Monthly Weather Review*, 132(2),  
662 405-421, 2004.

663 Mirschel, W., Wenkel, K.-O., Schultz, A., Pommerening, J., and Verch, G.: Dynamic  
664 phenological model for winter rye and winter barley. *European Journal of Agronomy*,  
665 23(2), 123-135, 2005.

666 Najeeb, U., Bange, M. P., Atwell, B. J., and Tan, D. K. Y.: Low Incident Light Combined  
667 with Partial Waterlogging Impairs Photosynthesis and Imposes a Yield Penalty in Cotton.  
668 *Journal of Agronomy and Crop Science*, 202(4), 331-341, 2016.

669 Newbery, F., Qi, A., and Fitt, B. D.: Modelling impacts of climate change on arable crop  
670 diseases: progress, challenges and applications. *Current Opinion in Plant Biology*, 32,  
671 101-109, 2016.

672 O'Brien, P., and Daigh, A.: Tillage practices alter the surface energy balance -A review.  
673 *Soil and Tillage Research*, 195, 2019.

674 Penuelas, J., Rutishauser, T., and Filella, I.: Phenology Feedbacks on Climate Change.  
675 *Science*, 324(5929), 887-888, 2009.

676 Reynolds, M., Foulkes, J., Furbank, R., Griffiths, S., King, J., Murchie, E., et al.:  
677 Achieving yield gains in wheat. *Plant Cell and Environment*, 35(10), 1799-1823, 2012.

678 Richardson, A. D., Keenan, T. F., Migliavacca, M., Ryu, Y., Sonnentag, O., and Toomey,  
679 M.: Climate change, phenology, and phenological control of vegetation feedbacks to the  
680 climate system. *Agricultural and Forest Meteorology*, 169, 156-173, 2013.

681 Sacks, W. J., Deryng, D., Foley, J. A., and Ramankutty, N.: Crop planting dates: an  
682 analysis of global patterns. *Global Ecology and Biogeography*, 19(5), 607-620, 2010.

683 Sacks, W. J., and Kucharik, C. J.: Crop management and phenology trends in the US  
684 Corn Belt: Impacts on yields, evapotranspiration and energy balance. *Agricultural and*  
685 *Forest Meteorology*, 151(7), 882-894, 2011.

686 Schillinger, W. F.: Rainfall Impacts Winter Wheat Seedling Emergence from Deep  
687 Planting Depths. *Agronomy Journal*, 103(3), 730, 2011.

688 Sellers, P. J., Tucker, C. J., Collatz, G. J., Los, S. O., Justice, C. O., Dazlich, D. A., et al.:  
689 A Revised Land Surface Parameterization (SiB2) for Atmospheric GCMS. Part II: The  
690 Generation of Global Fields of Terrestrial Biophysical Parameters from Satellite Data.  
691 *Journal of Climate*, 9(4), 706-737, 1996.

692 Seneviratne, S. I., Corti, T., Davin, E. L., Hirschi, M., Jaeger, E. B., Lehner, I., et al.:  
693 Investigating soil moisture-climate interactions in a changing climate: A review.  
694 *Earth-Science Reviews*, 99(3), 125-161, 2010.



695 Seneviratne, S. I., Phipps, S. J., Pitman, A. J., Hirsch, A. L., Davin, E. L., Donat, M. G.,  
696 et al.: Land radiative management as contributor to regional-scale climate adaptation and  
697 mitigation. *Nature Geoscience*, 11(2), 88-96, 2018.

698 Shi, P., Sun, s., Wang, M., Li, N., Wang, J., Jin, Y., et al.: Climate change regionalization  
699 in China (1961 - 2010)(In Chinese). *Science China: Earth Sciences*, 44(10), 2294-2306,  
700 2014.

701 Song, Y., Jain, A. K., and McIsaac, G. F.: Implementation of dynamic crop growth  
702 processes into a land surface model: evaluation of energy, water and carbon fluxes under  
703 corn and soybean rotation. *Biogeosciences*, 10(12), 8201-8201, 2013.

704 Tao, F., Yokozawa, M., and Zhang, Z.: Modelling the impacts of weather and climate  
705 variability on crop productivity over a large area: A new process-based model  
706 development, optimization, and uncertainties analysis. *Agricultural and Forest  
707 Meteorology*, 149(5), 831-850, 2009.

708 Tao, F. L., Zhang, S., Zhang, Z., and Rotter, R. P.: Maize growing duration was  
709 prolonged across China in the past three decades under the combined effects of  
710 temperature, agronomic management, and cultivar shift. *Global Change Biology*, 20(12),  
711 3686-3699, 2014.

712 Tao, F. L., Zhang, S. A., and Zhang, Z.: Spatiotemporal changes of wheat phenology in  
713 China under the effects of temperature, day length and cultivar thermal characteristics.  
714 *European Journal of Agronomy*, 43, 201-212, 2012.

715 Wuest, S. B.: Tillage depth and timing effects on soil water profiles in two semiarid soils.  
716 *Soil Science Society of America Journal*, 74(5), 1701-1711, 2010.

717 Wutzler, T., Lucas-Moffat, A., Migliavacca, M., Knauer, J., Sickel, K., Šigut, L., et al.:  
718 Basic and extensible post-processing of eddy covariance flux data with REddyProc.  
719 *Biogeosciences*, 15(16), 5015-5030, 2018.

720 Xiao, D. P., Moiwo, J. P., Tao, F. L., Yang, Y. H., Shen, Y. J., Xu, Q. H., et al.:  
721 Spatiotemporal variability of winter wheat phenology in response to weather and climate  
722 variability in China. *Mitigation and Adaptation Strategies for Global Change*, 20(7),  
723 1191-1202, 2015.

724 Xiao, D. P., and Tao, F. L.: Contributions of cultivars, management and climate change  
725 to winter wheat yield in the North China Plain in the past three decades. *European  
726 Journal of Agronomy*, 52, 112-122, 2014.

727 Xiao, D. P., Tao, F. L., Liu, Y. J., Shi, W. J., Wang, M., Liu, F. S., et al.: Observed  
728 changes in winter wheat phenology in the North China Plain for 1981-2009. *International  
729 Journal of Biometeorology*, 57(2), 275-285, 2013.

730 Yuan, L., Wang, E., Yang, X., and Jing, W.: Contributions of climatic and crop varietal  
731 changes to crop production in the North China Plain, since 1980s. *Global Change  
732 Biology*, 16(8), 2287-2299, 2010.

733 Zhang, X., Huang, G., Huang, Z., Bian, X., and Jiang, X.: Effects of low temperature on  
734 freezing injury of various winter wheat cultivars at different sowing time. *Agricultural  
735 Science & Technology*, 13(11), 2332-2337, 2012.

736 Zhang, X., Tang, Q., Zheng, J., Ge, Q., and Mao, R.: Suppression of spring rain by  
737 surface greening over North China Plain. *International Journal of Climatology*, 35(10),  
738 2752-2758, 2015.

739 Zhang, X. Z., Tang, Q. H., Zheng, J. Y., and Ge, Q. S.: Warming/cooling effects of  
740 cropland greenness changes during 1982-2006 in the North China Plain. *Environmental*  
741 *Research Letters*, 8(2), 2013.  
742